Pedestrian Guide to Symmetry Properties of the Reference Cubic Structure of 3D All-Inorganic and Hybrid Perovskites

ARTICLE *in* JOURNAL OF PHYSICAL CHEMISTRY LETTERS · JUNE 2015

Impact Factor: 7.46 · DOI: 10.1021/acs.jpclett.5b00905

1 AUTHOR:

J. Even
Institut National des Sciences Appliquées de R…

334 PUBLICATIONS **1,640** CITATIONS

SEE PROFILE

THE JOURNAL OF PHYSICAL CHEMISTRY Letters

Viewpoint

pubs.acs.org/JPCL

Pedestrian Guide to Symmetry Properties of the Reference Cubic Structure of 3D All-Inorganic and Hybrid Perovskites

A scientific breakthrough toward possible industrialization of hybrid organic perovskites (HOPs) was achieved in the last 3 years with 3D HOPs in the field of photovoltaics.[1−11] The understanding of the basic properties of HOPs remains rather scanty, despite intense efforts devoted to density functional theory studies by many theoretical groups (see an almost exhaustive list of theoretical papers from 2013/2014 in ref 12). A general approach of 3D HOPs based on solid-state physics concepts already developed in the field of IV, II−V, or II−VI semiconductors is nevertheless possible.[12−19] For the conventional semiconductors, progress in industrial applications and fundamental physics has been made almost in parallel over the last century.[13,14] Knowledge has often profited from semiempirical approaches based on basic solid-state physics concepts and symmetry considerations. In order to capture the main physics in the new "class" of semiconductors, we recently proposed considering the high-temperature 3D HOP pseudocubic phase as a reference.[12,17] Considering a highly symmetric phase as a reference as well as using symmetry analyses and a empirical Hamiltonian has many advantages, and some aspects have already been preliminary explored to some extent for HOPs but also all-inorganic halide perovskites (AIPs).[17,20] The most important problem for DFT simulations of HOPs in the high-temperature phases is related to the dynamical disorder of the organic cations.[21−23] The aim of this Viewpoint is thus to show that a rigorous symmetry analysis is nevertheless possible. The symmetry properties of the *Pm*-3*m* cubic phase of AIPs or the disordered pseudocubic *Pm*-3*m* phase of 3D HOPs are introduced step by step for that purpose.[24,25] It will help rigorously exploit results in the field of DFT where group theory has been seldom used. A bunch of DFT simulations were indeed designed in the past to describe the electronic and structural properties of HOP phases[12] but sometimes breaking the symmetries of these phases and therefore questioning the validity of theoretical predictions. The interpretation of experiments dedicated to the electronic or optical properties of AIPs and HOPs may also greatly benefit from symmetry analyses. Valuable recent attempts to simulate the disorder in HOP materials by molecular dynamics may be also hampered by finite size effects or implicit symmetry breaking related to particular supercell choice.[26−28] Brute force, and thus computationally demanding, theoretical approaches, as well as ongoing structural studies, could be efficiently combined with group symmetry analyses and interpreted on the basis of the pseudospin concept.

Figure 1a represents the real space 3D view of the *Pm*-3*m* crystal structure of metal halide AMX_3 perovskites, where A can be an inorganic or organic cation, M a metal, and X a halogen.

At high temperature, experimental crystal structures of HOPs do not reveal strictly ordered and symmetric phases as a consequence of molecular symmetry of the organic cations that do not fit the site symmetry of the lattice. Related dynamical disorder was already analyzed a long time ago by various experimental techniques.[21−23] Nevertheless, their reference high-temperature phase can be taken as being the *Pm*-3*m* cubic phase, for example, that of $CsPbX_3$ ($Z = 1$). In 3D HOPs, the positions of individual atoms of the organic cation are dynamically averaged and occupy the same special Wickoff position at the center of the cubic cell. The *Pm*-3*m* space group severely restricts the symmetries and multiplicities of the species located at (0,0,0) (M, 1a), (1/2,1/2,1/2) (A, 1b), and (1/2,0,0) (X, 3d) sites. In order to rigorously take into account both the *Pm*-3*m* lattice symmetry and the thermally activated disorder associated with the tumbling of the organic cations, we split the degrees of freedom of molecular cations A located at site 1b in two parts, (i) translations of the molecular center of mass and electric monopole (CM) and (ii) rotations of the molecular axis around position (1/2,1/2,1/2), for instance, rotation of the C−N axis when A = $CH_3NH_3^+$ (oriented electric dipole). Additional degrees of freedom related to hydrogens also play a role in determining the possible orientations. Regarding electronic properties of HOPs, replacement of the molecular cation by a Cs^+ located at the molecular CM accurately mimics the ionic interactions due to the electric monopole and affords reliable band diagrams and related properties.[15−19] However, steric effects, atomic motion, and molecular tumbling are crucial to understand crystal packing of HOPs, phase transitions, and optoelectronic properties. Besides, separation of the molecular translational and rotational degrees of freedom neglects the linear rotational−vibrational coupling in the lattice. This coupling is allowed by symmetry in the cubic phase, as shown later, and could be reconsidered in a second step, but this is beyond the scope of this simplified presentation. This approximation however no longer applies in the low-temperature phase. The *Pm*-3*m* space group is a symmorphic space group.[25] Its symmetry operations rely on the 48 symmetry operations of the

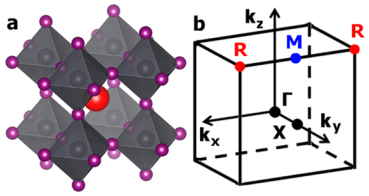

Figure 1. (a) Real space 3D view of the *Pm*-3*m* reference cubic crystal structure of metal halide AIPs or HOPs of general formula AMX_3, where A is an inorganic cation or an organic cation such as $CH_3NH_3^+$, M a metal, and X a halogen. In HOPs, the $CH_3NH_3^+$ cation is located at the center of the cube with an averaged position sketched by the red ball. (b) Reciprocal space 3D view showing the first Brillouin zone (BZ) of the *Pm*-3*m* space group. Points of high symmetry in the cubic BZ are indicated by conventional letters; Γ denotes the origin of the BZ, X is the center of a square face at the BZ boundary, M is a center of a cube edge, and R are vertices of the cube. Reprinted with permission from ref 18. Copyright 2014 American Chemical Society.

Published: June 18, 2015

DOI: 10.1021/acs.jpclett.5b00905
J. Phys. Chem. Lett. 2015, 6, 2238−2242

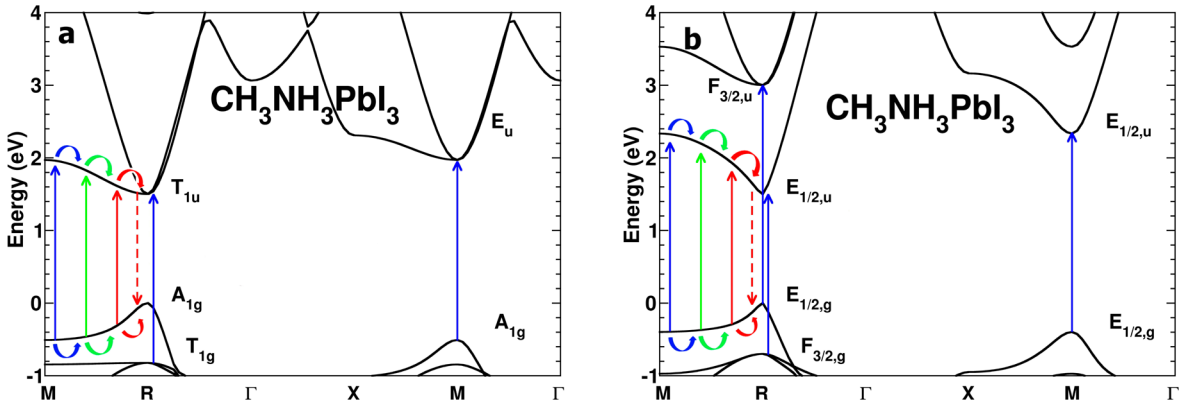

Figure 2. Electronic band structure for the high-temperature cubic *Pm*-3*m* phase of $CH_3NH_3PbI_3$ without (a) and with (b) SOC at the LDA (local density approximation) level of theory. Upward energy shifts of 0.3 (a) and 1.4 eV (b) have been applied to match the experimental band gap value at R. Labels of IRs obtained from simple (a) and double (b) group representations are given at R and M for electronic states close to the band gap (see Tables S1 and S2, Supporting Information). Vertical arrows show various possible optical transitions close to the band gap energy. Optical transitions along the M−R line generate carriers that can relax easily toward R. Reprinted with permission from ref 18. Copyright 2014 American Chemical Society.

O_h ($m3m$) point group and the translational symmetries of the cubic lattice. Among the point group symmetries, inversion plays an important role, yielding either symmetric (g) or antisymmetric (u) irreducible representations (IRs) of the symmetry group (Tables S1 and S2, Supporting Information). Translational symmetry of the lattice must be used to analyze collective excitations. It is thus necessary in many cases to switch to a reciprocal space representation of the lattice symmetries.[12,18] Figure 1b shows the reciprocal space 3D view of the first BZ of the *Pm*-3*m* space group, with some points of high symmetry.[18] Reciprocal lattice vectors $\mathbf{K}_m$ are related to the translational periodicity of the reciprocal lattice, thus enabling a representation of the various lattice properties within the first BZ. It is, for example, useful to describe the electronic energy eigenfunctions as Bloch waves[12−15]

$$\psi_{n,\mathbf{k}}(\mathbf{r}) = e^{i\mathbf{k}\cdot\mathbf{r}} u_{n,\mathbf{k}}(\mathbf{r}) \quad (1)$$

where n is the band index, $\mathbf{r}$ the position vector, $\mathbf{k}$ the wave vector inside of the BZ, and $u_{n,\mathbf{k}}(\mathbf{r})$ the periodic part of the eigenfunction. The center of the BZ Γ(0,0,0) and R(1/2,1/2,1/2) are special high-symmetry $\mathbf{k}$ points of the first BZ that play an important role in the physical properties of AIPs and HOPs. For both points, the group of the wave vector is O_h, and many lattice properties of HOPs can be analyzed using the character tables of the IRs of the O_h point group (Tables S1 and S2, Supporting Information).

In order to account for the site symmetry, in the perovskite cubic lattice, it is necessary to compute first its site-reducible representation χ_{site}. At the Γ point, the site symmetries correspond to the Γ_1^+, $\Gamma_1^+ + \Gamma_3^+$, Γ_1^+ for M, X, and A, respectively. Then, from the reducible representation χ_{phys} describing a given onsite atomic or molecular physical parameter (atomic displacement or orbital, molecular pseudospin or static orientation, etc.), one may deduce the corresponding physical representation within the lattice by computing the product $\chi_{site} \otimes \chi_{phys}$. If one reduces the A molecule to an electric dipole, molecular symmetry would be described by $\chi_{phys} = \Gamma_4^-$, which is incompatible with the lattice symmetry because $\chi_{site} \otimes \chi_{phys} = \Gamma_1^+ \otimes \Gamma_4^- = \Gamma_4^-$ does not contain the crystal totally symmetric representation Γ_1^+. For that reason, molecular orientations are necessarily disordered when taking lattice periodicity into account.

It is well-known that close to the band gap of HOPs, optical transitions involve mainly s and p orbitals of the metal M and p orbitals of halogen X. The corresponding electronic band structures are usually plotted within the BZ (Figure 2a). Leaving aside for a moment spin−orbit coupling (SOC), the possible symmetrized linear combinations of atomic orbitals (SLCAO) can be inferred from symmetry. At Γ, SLCAO leads to Γ_1^+, Γ_4^-, and $2\Gamma_4^- + \Gamma_5^-$ IRs for s(M), p(M), and p(X) orbitals, respectively. This simple analysis shows that totally symmetric Γ_1^+ s(M)−p(X) hybridization is forbidden at Γ. A similar analysis at R yields R_1^+, R_4^-, and $R_1^+ + R_3^+ + R_4^+ + R_5^+$, IRs for s(M), p(M), and p(X) orbitals, respectively. The totally symmetric R_1^+ (A_{1g}) obviously correspond to s(M)−p(X) hybridized atomic orbitals at the top of the valence band (VBM) at point R.[18] Meanwhile, the vectorial representation R_4^- (T_{1u}) relevant for the bottom of the conduction band (CBM) at R involves hybridization between p(M) orbitals. Regardless of the crystal structure, a giant SOC operates on the CB of lead-based AIPs[17,20] and HOPs[15,16] (Figure 2b). Analysis of $CH_3NH_3MX_3$ compounds (M = Pb, Sn, Ge) shows that SOC splitting of the CBM is consistent with metal atomic energy level tables.[17,19] Applying symmetry considerations while considering electron spin effects (e.g., SOC) requires double groups.[18,24,25] Double space group IRs are deduced from the products of the $D_{1/2} = E_{1/2g}$ electron spin IRs with the simple space group IRs. Bloch functions transform as IRs of the double space group, whose character table is given in Table S2 (Supporting Information) for *Pm*-3*m*. CBM becomes a two-fold-degenerate spin−orbit split-off (SO) state as SOC leads to a large energy splitting. The remaining four-fold-degenerate CB states undergo a positive energy shift. In other words, the simple group R_4^- vectorial representation of the CBM at R splits in a doubly degenerate R_6^- ($E_{1/2u}$) SO state and a four-fold-degenerate R_8^- ($F_{3/2u}$), light (LE) and heavy (HE) electron states (Figure 2b).[18] Light and heavy terms are used in reference to the effective masses away from R. Time reversal symmetry is important for spin effects and yields the general conditions for conjugated spinor states, $E_n\uparrow(\mathbf{k}) = E_n\downarrow(-\mathbf{k})$ and $E_n\downarrow(\mathbf{k}) = E_n\uparrow(-\mathbf{k})$. Inversion symmetry in *Pm*-3*m* structure yields additional conditions: $E_n\uparrow(\mathbf{k}) = E_n\uparrow(-\mathbf{k})$ and $E_n\downarrow(\mathbf{k}) = E_n\downarrow(-\mathbf{k})$. Combining both symmetries leads to a double spin degeneracy $E_n\uparrow(\mathbf{k}) = E_n\downarrow(\mathbf{k})$ across all of the dispersion

DOI: 10.1021/acs.jpclett.5b00905
J. Phys. Chem. Lett. 2015, 6, 2238−2242

diagram within the BZ. Indeed, all of the double group IRs at Γ and R are two- or four-dimensional (Table S2, Supporting Information).

Symmetry analysis of the electronic states at the R point of the BZ allow identification of optically allowed transitions.[18] The selection rules derive from the direct product of CB and VB IRs, which must contain the photon operator IR (T_{1u}). When SOC is neglected, this condition is fulfilled at the band gap of HOPs and AIPs for spinless states because $T_{1u} \otimes A_{1g} = T_{1u}$ (Figures 2a and 3).[18] Excitons are related to additional

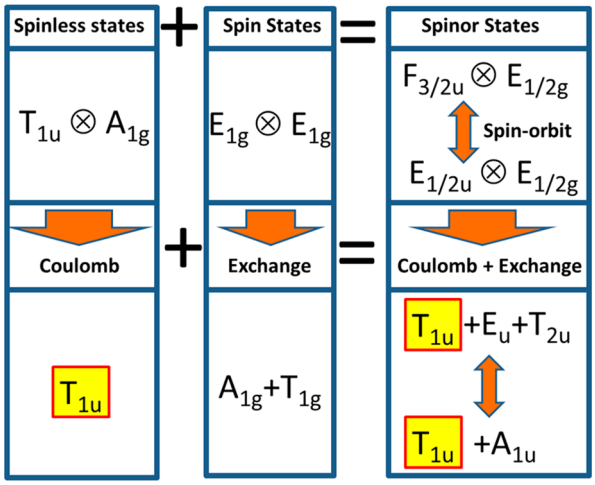

Figure 3. Symmetry representations of the CB and VB pair states leading to optically allowed transitions. Pure spinless and spin states are considered, as well as combined spinor states. The influences of SOC, Coulomb, and exchange interactions are illustrated. Excitonic states leading to optically allowed transitions are indicated in yellow.

Coulomb interactions between electrons and holes in a Wannier picture.[18,29,30] The possible symmetries of these excitons result from the direct product of the simple group IRs of the relevant CB state, VB state, and envelope function. For the exciton ground state at R with an S-type envelope function (A_{1g}), the $T_{1u} \otimes A_{1g} \otimes A_{1g}$ product yields the IR of the exciton ground state T_{1u} (Figure 3). The optical transition from the excitonic ground state to the crystal ground state A_{1g} is allowed because the IR product of the exciton and the photon operator contains the crystal ground-state IR. When considering only the spin of the particles, the electron and hole pure spin states form singlet (S = 0) and triplet (S = 1) states $A_{1g} + T_{1g}$, usually separated by an exchange energy (Figure 3). When the SOC is negligible, it is often possible to use directly these two analyses to account for the effects of Coulomb and exchange interactions on the optical transitions. In the case of AIPs and HOPs, however, the SOC is larger than the Coulomb and exchange interactions, and a better starting point is afforded by spinor states (Figure 3). The ground-state isotropic optical transition stems from the transition between the doubly degenerate $E_{1/2g}$ VBM and $E_{1/2u}$ CBM states. At R, a series of other transitions are optically allowed (Figure 2b),[18] involving, for example, pair states associated with the LE and HE states of the CB $F_{3/2u}$ double group IR (Figures 2b and 3).

Vibrations of a crystal lattice correspond to degrees of freedom that can be studied in the harmonic approximation of small displacements. The vectorial representation of the O_h group for all of the atomic displacements is $\chi_{phys} = T_{1u}$. For vibrational modes at the Γ point, M, A, and 3X yield Γ_4^-, Γ_4^-, and $2\Gamma_4^- + \Gamma_5^-$, respectively (Figure 4).[18,31] The three acoustic modes belong to Γ_4^-, whereas the 12 optical phonons correspond to the $3\Gamma_4^- + \Gamma_5^-$ IR.

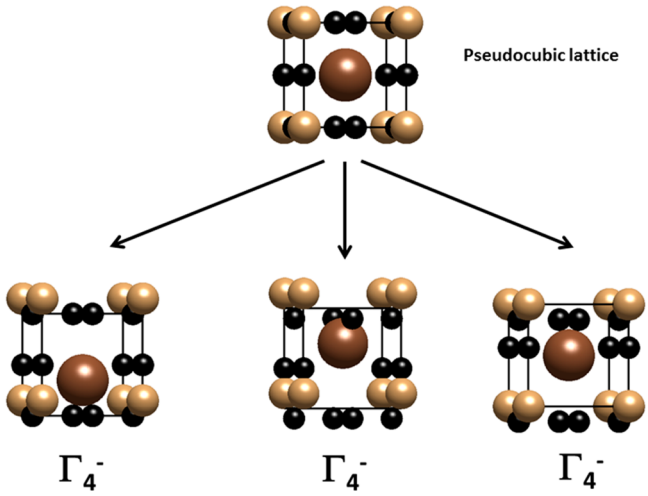

Figure 4. Zone center Γ_4^- optical phonon modes of AMX_3 AIPs[31] or HOPs[18] in ideal cubic crystal perovskite structure with space group *Pm*-3*m*. Vibrations along only the vertical direction of each triply degenerate mode are schematically presented. The motions of the M and X atoms and the sphere representing the A atom in AIPs or the molecular CMs in HOPs are shown by comparison to the equilibrium at the top. IRs can be also labeled according to the O_h point group IR $T_{1u}(\Gamma_4^-)$.

Early millimeter wave spectroscopy, NMR, and dielectric measurements have shown that close to room-temperature $CH_3NH_3^+$ is tumbling between various dipole orientations.[21−23] Such a behavior could be investigated by molecular dynamics.[26−28] Here, we proceed with a symmetry-based analysis that incorporates both the intrinsic disorder and translational symmetry of the lattice. The three simplest scenarios (A, B, and C) correspond to the simplest sets of unit vectors and have been suggested earlier to rationalize the influence of molecular disorder in phase transition.[21,22] In scenarios A, B, and C, the molecular dipole points toward a cubic cell facet, a halogen atom, or the center of an octahedron, respectively. However, experimental investigations (calorimetry, X-ray diffraction) did not allow differentiating clearly the role played by each scenario in the high-temperature phase of HOPs. The molecular orientations (C−N axis) may be described by a discrete pseudospin variable for each molecule that is equal to 1 for a given orientation and 0 for all others. When all molecular configurations are considered, the general pseudospin state for scenario A is a six-fold vector

$$\begin{vmatrix} N_1 \\ N_2 \\ N_3 \\ N_4 \\ N_5 \\ N_6 \end{vmatrix}$$

where N_i is the occupation number of one of the six {1,0,0} orientations. The model thus incorporates in a simple way the thermally activated disorder of the molecular orientations in a

DOI: 10.1021/acs.jpclett.5b00905
J. Phys. Chem. Lett. 2015, 6, 2238−2242

local cubic environment and symmetry. At the Γ point, the totally symmetric representation Γ_1^+ shows up in each pseudospin decomposition, yielding the same occupation probability for all of the orientations (Figure 5). These

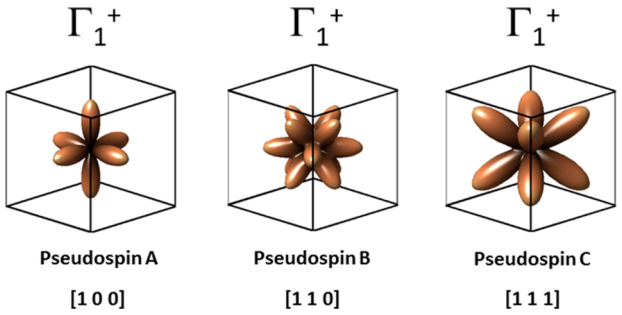

Figure 5. Schematic representations of the totally symmetric IR representations Γ_1^+ for the three pseudospins corresponding to [100], [110], or [111] molecular orientations. Each lobe is proportional to an occupation number along a particular orientation. For totally symmetric IR representations of pseudospins, the occupation probability is the same for all of the orientations.

configurations are nonpolar and correspond to the concept of an elastic totally symmetric multipole. In other words, it allows simultaneously taking into account the dynamical disorder and steric interactions. Noteworthy, it shows that a representation of the molecular disordered configurations in a cubic environment by spheres (effective atoms for example) is a crude approximation. The deviations of the occupation numbers from the Γ_1^+ steady-state solutions are defined as $\boldsymbol{n}_i$ with $\sum_i \boldsymbol{n}_i = 0$. Allowed symmetrized combinations of these deviations define the possible pseudospin excitation modes of the system. At the Γ point, the IR decomposition reads, for example, $\Gamma_1^+ + \Gamma_3^+ + \Gamma_5^+ + \Gamma_4^- + \Gamma_5^-$ for scenario B. Nonpolar even configurations like $\Gamma_3^+ + \Gamma_5^+$ correspond to elastic multipoles, while polar and odd configurations like $\Gamma_4^- + \Gamma_5^-$ correspond to electric multipoles.

Let us conclude this Viewpoint by describing with a few examples how cubic symmetry breaking may affect the physical properties of AIPs and HOPs. At a first sight, the electronic band structure of the *Pnma* phase of $CH_3NH_3PbI_3$ appears very different from that of the reference cubic phase. The effect of the *Pm*-3*m* to *Pnma* cell transformation can be explored considering a $(\vec{a} + \vec{b}, 2\vec{c}, \vec{a} - \vec{b})$ supercell of the cubic lattice while keeping the atoms at the special positions of the *Pm*-3*m* phase.[12,19] As the cell size undergoes a four-fold increase, it leads to a reduction of the BZ volume by the same amount. Electronic states close to the band gap are folded from R of the *Pm*-3*m* BZ to Γ of the *Pnma* supercell BZ. This band folding clarifies the seeming complexity of the band diagram in the low-temperature phase. This procedure reveals that, besides electronic band folding, the most important transformation of the diagram is due to atomic displacements and strain.[12,19] Similar band folding helps to understand the main features of the electronic band diagram of the *Pm*-3*m* to *I*4*mcm* cell transformation or other transformations.[12] Loss of inversion symmetry is also a possible consequence of a phase transition or local strain. Time reversal symmetry is still active, but the spin degeneracy condition $E_n\uparrow(\mathbf{k}) = E_n\downarrow(\mathbf{k})$ is usually lost for a general wave vector, except for special high-symmetry points.[17,32] In 3D HOPs, it has been shown early that even a small inversion symmetry breaking can lead to a strong spinor splitting because the SOC effect is giant as compared to conventional semiconductors.[17] Indeed, the electronic band diagram of the *P*4*mm* phase of $CH_3NH_3MI_3$ close to the critical point A of the BZ (corresponding to R of *Pm*-3*m*) exhibits a splitting of the spinor bands, even though the deviation from the centrosymmetric *Pm*-3*m* phase is small. This effect is more important for the tetragonal *I*4*cm* phase.[17] Such a **k**-dependent band splitting, also designated under the Rashba/Dresselhaus, Dresselhaus, and Rashba effect, was confirmed by many theoretical groups[33,34] but still deserves experimental evidence in HOPs.

J. Even*

Fonctions Optiques pour les Technologies de l'Information, FOTON UMR 6082, CNRS, INSA de Rennes, 35708 Rennes, France

■ ASSOCIATED CONTENT

Supporting Information

Character table of the IR of the O_h point groups and *Pm*-3*m* space groups at Γ and R points of the BZ. The Supporting Information is available free of charge on the ACS Publications website at DOI: 10.1021/acs.jpclett.5b00905.

■ AUTHOR INFORMATION

Corresponding Author

*E-mail: Jacky.Even@insa-rennes.fr. Tel: +33 (0)2 23 23 82 95. Fax: +33 (0)2 23 23 86 18.

Notes

The authors declare no competing financial interest.

■ ACKNOWLEDGMENTS

The author would like to thank Dr. Claudine Katan for fruitful discussions.

■ REFERENCES

(1) Kojima, A.; Teshima, K.; Shirai, Y.; Miyasaka, T. Organometal halide perovskites as visible-light sensitizers for photovoltaic cells. *J. Am. Chem. Soc.* **2009**, *131*, 6050−6051.

(2) Im, J.-H.; Lee, C.-R.; Lee, J.-W.; Park, S.-W.; Park, N.-G. 6.5% efficient perovskite quantum-dot-sensitized solar cell. *Nanoscale* **2011**, *3*, 4088−4093.

(3) Lee, M. M.; Teuscher, J.; Miyasaka, T.; Murakami, T. N.; Snaith, H. J. Efficient hybrid solar cells based on meso-superstructured organometal halide perovskites. *Science.* **2012**, *338*, 643−647.

(4) Kim, H.-S.; Lee, C. R.; Im, J. H.; Lee, K. B.; Moehl, T.; Marchioro, A.; Moon, S. J.; Humphry-Baker, R.; Yum, J. H.; Moser, J. E.; Grätzel, M.; Park, N. G. Lead iodide perovskite sensitized all-solid-state submicron thin film mesoscopic solar cell with efficiency exceeding 9%. *Sci. Rep.* **2012**, *2*, 591/1−591/7.

(5) Nie, W.; Tsai, H.; Asadpour, R.; Blancon, J.-C.; Neukirch, A.; Gupta, G.; Crochet, J. J.; Chhowalla, M.; Tretiak, S.; Alam, M. A.; Wang, H.-L.; Mohite, A. High-efficiency solution-processed perovskite solar cells with millimeter-scale grains. *Science* **2015**, *347*, 522−525.

(6) Park, N. G. Organometal perovskite light absorbers toward a 20% efficiency low-cost solid-state mesoscopic solar cell. *J. Phys. Chem. Lett.* **2013**, *4*, 2423−2429.

(7) Snaith, H. J. Perovskites: The emergence of a new era for low-cost, high-efficiency solar cells. *J. Phys. Chem. Lett.* **2013**, *4*, 3623−3630.

(8) Kim, H. S.; Im, S. H.; Park, N.-G. Organolead halide perovskite: New horizons in solar cell research. *J. Phys. Chem. C* **2014**, *118*, 5615−5625.

(9) Gao, P.; Graëtzel, M.; Nazeeruddin, M. K. Organohalide lead perovskites for photovoltaic applications. *Energy Environ. Sci.* **2014**, *7*, 2448−2463.

DOI: 10.1021/acs.jpclett.5b00905
J. Phys. Chem. Lett. 2015, 6, 2238−2242

(10) Gonzalez-Pedro, V.; Juarez-Perez, E. J.; Arsyad, W.-S.; Barea, E. M.; Fabregat-Santiago, F.; Mora-Sero, I.; Bisquert, J. General working principles of $CH_3NH_3PbX_3$ perovskite solar cells. *Nano Lett.* **2014**, *14*, 888−893.
(11) *Best research-cell efficiencies*. http://www.nrel.gov/ncpv/images/efficiency_chart.jpg (2015).
(12) Even, J.; Pedesseau, L.; Katan, C.; Kepenekian, M.; Lauret, J.-S.; Sapori, D.; Deleporte, E. Solid-State Physics Perspective on Hybrid Perovskite Semiconductors. *J. Phys. Chem. C* **2015**, *119*, 10161−10177.
(13) Chuang, S. In *Physics of Optoelectronic Devices*; Goodman, J. W., Ed.; Wiley: New York, 1995.
(14) Yu, P. Y.; Cardona, M. *Fundamentals of Semiconductors*, 3rd ed.; Springer: Berlin, Heidelberg, Germany; New York, 2005.
(15) Even, J.; Pedesseau, L.; Dupertuis, M.-A.; Jancu, J.-M.; Katan, C. Electronic model for self-assembled hybrid organic/perovskite semiconductors: Reverse band edge electronic states ordering and spin−orbit coupling. *Phys. Rev. B* **2012**, *86*, 205301.
(16) Even, J.; Pedesseau, L.; Jancu, J.-M.; Katan, C. Importance of spin−orbit coupling in hybrid organic/inorganic perovskites for photovoltaic applications. *J. Phys. Chem. Lett.* **2013**, *4*, 2999−3005.
(17) Even, J.; Pedesseau, L.; Jancu, J.-M.; Katan, C. DFT and k • p modelling of the phase transitions of lead and tin halide perovskites for photovoltaic cells. *Phys. Status Solidi RRL* **2014**, *8*, 31−35.
(18) Even, J.; Pedesseau, L.; Katan, C. Analysis of multivalley and multibandgap absorption and enhancement of free carriers related to exciton screening in hybrid perovskites. *J. Phys. Chem. C* **2014**, *118*, 11566−11572.
(19) Katan, C.; Pedesseau, L.; Kepenekian, M.; Rolland, A.; Even, J. Interplay of spin−orbit coupling and lattice distortion in metal substituted 3D tri-chloride hybrid perovskites. *J. Mater. Chem. A* **2015**, *3*, 9232−9240.
(20) Jin, H.; Im, J.; Freeman, A. J. Topological insulator phase in halide perovskite structures. *Phys. Rev. B* **2012**, *86*, 121102(R).
(21) Poglitsch, A.; Weber, D. Dynamic disorder in methylammoniumtrihalogenoplumbates (II) observed by millimeter-wave spectroscopy. *J. Chem. Phys.* **1987**, *87*, 6373−6378.
(22) Onoda-Yamamuro, N.; Matsuo, T.; Suga, H. Dielectric study of $CH_3NH_3PbX_3$ (X = Cl, Br, I). *J. Phys. Chem. Solids* **1992**, *53*, 935−939.
(23) Wasylishen, R. E.; Knop, O.; Macdonald, J. B. Cation rotation in methylammonium lead halides. *Solid State Commun.* **1985**, *56*, 581−582.
(24) Altmann, S. L.; Herzig, P. *Point-Group Theory Tables*; Clarendon: Oxford, U.K., 1994.
(25) Miller, S. C.; Love, W. F. *Tables of Irreducible Representations of Space Groups and Co-Representations of Magnetic Space Groups*; Preutt: Boulder, CO, 1967.
(26) Mosconi, E.; Quarti, C.; Ivanovska, T.; Ruani, G.; De Angelis, F. Structural and electronic properties of organo-halide lead perovskites: A combined IR-spectroscopy and ab initio molecular dynamics investigation. *Phys. Chem. Chem. Phys.* **2014**, *16*, 16137−16144.
(27) Lindblad, R.; Bi, D.; Park, B.-W.; Oscarsson, J.; Gorgoi, M.; Siegbahn, H.; Odelius, M.; Johansson, E. M. J.; Rensmo, H. Electronic structure of $TiO_2/CH_3NH_3PbI_3$ perovskite solar cell interfaces. *J. Phys. Chem. Lett.* **2014**, *5*, 648−653.
(28) Carignano, M. A.; Kachmar, A.; Hutter, J. Thermal effects on $CH_3NH_3PbI_3$ perovskite from ab initio molecular dynamics simulations. *J. Phys. Chem. C* **2015**, *119*, 8991−8997.
(29) Fang, H.-H.; Raissa, R.; Abdu-Aguye, M.; Adjokatse, S.; Blake, G. R.; Even, J.; Loi, M. A. Photophysics of organic−inorganic hybrid lead iodide perovskite single crystals. *Adv. Funct. Mater.* **2015**, *25*, 2378.
(30) Tanaka, K.; Takahashi, T.; Ban, T.; Kondo, T.; Uchida, K.; Miura, N. Comparative study on the excitons in lead-halide-based perovskite type crystals $CH_3NH_3PbBr_3$ $CH_3NH_3PbI_3$. *Solid State Commun.* **2003**, *127*, 619−623.
(31) Hua, G. L. Normal vibration modes and the structural phase transitions in cesium trichloroplumbate $CsPbCl_3$. *J. Phys.: Condens. Matter* **1991**, *3*, 1371.
(32) Winkler, R. *Spin−Orbit Coupling Effects in Two-Dimensional Electron and Hole Systems*; Tracts in Modern Physics; Springer-Verlag: New York, 2004.
(33) Roiati, V.; Mosconi, E.; Listorti, A.; Colella, S.; Gigli, G.; De Angelis, F. Stark effect in perovskite/TiO_2 solar cells: Evidence of local interfacial order. *Nano Lett.* **2014**, *14*, 2168−2174.
(34) Kim, M.; Im, J.; Freeman, A. J.; Ihm, J.; Jin, H. Switchable $S = 1/2$ and $J = 1/2$ Rashba bands in ferroelectric halide perovskites. *Proc. Natl. Acad. Sci. U.S.A.* **2014**, *111*, 6900−6904.

DOI: 10.1021/acs.jpclett.5b00905
J. Phys. Chem. Lett. 2015, 6, 2238−2242